Journal of Physics: Conference Series **689** (2016) 012023 doi:10.1088/1742-6596/689/1/012023

Probing ultrafast processes by fifth order Stimulated Raman Scattering

G Fumero[1], G Batignani[1,2], K E Dorfman[3], S Mukamel[3], T Scopigno[1,4]

[1] Dipartimento di Fisica, Università di Roma "La Sapienza", I-00185, Roma, Italy
[2] Dipartimento di Scienze Fisiche e Chimiche, Università degli Studi dell'Aquila, I-67100, L'Aquila, Italy
[3] Department of Chemistry, University of California, California 92697-2025, Irvine, USA
[4] Center for Life Nano Science @Sapienza, Istituto Italiano di Tecnologia, 295 Viale Regina Elena, I-00161, Roma, Italy

E-mail: giuseppe.fumero@gmail.com, tullio.scopigno@phys.uniroma1.it

Abstract. We present the full diagrammatic description of non-resonant impulsive femtosecond stimulated Raman spectroscopy in a multimode model system. In this technique the pump-probe scheme is exploited to study the vibrational structure of the sample via stimulated Raman scattering. We apply closed-time-path-loop diagrams to calculate the complete response of the system at the relevant perturbation order. We show that, in presence of low-frequency modes, coherences created by the impulsive pump modify the resulting Raman signal, which oscillates from gain to loss features, depending on the time delay between the pump and probe pulses. This leads to a redistribution of photons among the fields involved in the process and, consequently, the energy flows between fields and matter. Moreover, through this formalism, we address the case of extremely short delays in which the pump and probe fields overlap in time. We find that, even in absence of photo-induced dynamics due to absorption of the pump pulse, the overlap condition can generate time dependent features, arising from additional diagrams, which offer no contribution for well separated pulses.

1. Introduction

Ultrafast spectroscopy has recently emerged as a key tool in scientific inquiry, due to its capability to probe picosecond and sub-picosecond time scales at which atomic and molecular systems evolve. Revealing dynamics that last for extremely short amounts of time has a central role in the understanding of many fundamental and unknown phenomena that appear in numerous fields, from solid state physics to biochemistry [1–4].

The investigation of such dynamics, however, implies deciphering complex signals and requires a careful modeling to extract the information brought by the experimental measurements. The need for a powerful theoretical method to understand such signals has motivated the application of several perturbative techniques to spectroscopic problems and, in particular, to nonlinear spectroscopy [5]. Generally, nonlinear optical processes are described by the density matrix of the matter system interacting with light, while electromagnetic degrees of freedom are treated classically, through the Maxwell equations. The nonlinear signature of the process is contained in the induced polarization, which is calculated starting from the density matrix and acts as source in the Maxwell equations.

Specifically, a perturbative expansion in power of the fields leads the nth order polarization $P^{(n)}$, which describes $n+1$ light matter interactions, including the emission of the nonlinear signal. The full response is calculated summing all the possible orderings of the fields interactions and, consequently, all the possible pathways of the density matrix in its configuration space, called Liouville space. This is easily achieved through diagrammatic representations. Perturbation expansions based on the density matrix are represented by double-sided Feynman diagrams: the two sides of the diagram represent the ket and bra sides of the density matrix, while the arrows stand for excitations or de-excitations induced by the fields.
Another possibility consists in founding the perturbative expansion on the wave function of the complete system, coupling both the matter and the fields degrees of freedom quantum-mechanically. A different diagrammatic representation is then supplied by closed-time path-loop diagrams [6, 7], which describe the evolution of the wave function both forward and backwards in real time. This method allows for a dramatic reduction of the perturbative terms, since the number of loop diagrams scales linearly with n, while fully time ordered Feynman diagrams scale as n^2.
Here we apply loop diagrams to provide a full quantum description of non resonant Femtosecond Stimulated Raman Scattering (nr-FSRS) [8, 9]. This technique uses an ultrashort non resonant actinic pulse to create coherences of low-frequecy modes in the sample. The state of the system is then probed stimulating a Raman process through another mode of the system, using a narrowband Raman pulse and a broadband probe pulse. When the pump and probe pulses do not overlap in time, we find a modulation of the Raman signal, due to the actinic-induced low-frequecy coherences, in agreement with previous works [8, 10]. Additionally, our approach allows the microscopic tracking of the energy redistribution among fields and matter during the process. Moreover, we investigate the case of extremely short delay times between the pump and probe pulses. We demonstrate that in this instance additional terms have to be considered in the perturbative expansion.

2. The perturbative approach to non resonant FSRS

The nonlinear optical process underlying nr-FSRS is ruled by the Hamiltonian

$$H = H_0 + H', \tag{1}$$

where the unperturbed Hamiltonian H_0 is separable in a matter and an electromagnetic contribution, H_m and H_f respectively, and all its eigenfuctions are assumed to be known. The interaction term H' represents the effective radiation matter interaction. Assuming off-resonant excitations, the effective interaction Hamiltonian in the rotating wave approximation is given by

$$H'(t) = \alpha(t) \sum_{i,j} \mathcal{E}_j^\dagger(t)\mathcal{E}_i(t) + h.c. \tag{2}$$

where $\mathcal{E}_i$ and $\mathcal{E}_j^\dagger$ are the positive and negative frequency components for two different modes i and j of the field operator

$$\hat{E}(\mathbf{r}, t) = \sum_j \mathcal{E}_j(t) e^{i\mathbf{k_j}\cdot\mathbf{r}} + \sum_j \mathcal{E}_j^\dagger(t) e^{-i\mathbf{k_j}\cdot\mathbf{r}}. \tag{3}$$

In nr-FSRS experiments, the total field comes from the sum of the actinic pulse (E_a), Raman pump (E_p) and probe (E_s) fields. Since all the laser pulses are far from the resonance frequencies of the sample, excitations to virtual levels are ruled by the excited state polarizability operator

$$\alpha = \sum_{a \neq b} \alpha_{ab} \left|a\right\rangle \left\langle b\right|. \tag{4}$$

Although, as a matter of principle, the i and j run over all the possible modes of the total field operator $\hat{E}$, the energy and momentum conservation, as well as the experimental configuration of the pulses, limit this freedom and reduce the number of terms contributing to the signal in the summation. The stimulated signal is defined as the change in time of the mean number of photons $n_\omega(t)$ in the detected mode ω, belonging to the probe pulse E_s:

$$S = \int_{-\infty}^{+\infty} dt \frac{d}{dt} \left\langle n_\omega(t) \right\rangle = \int_{-\infty}^{+\infty} dt \frac{i}{\hbar} \left\langle \left[H', n_\omega(t) \right] \right\rangle = \frac{2}{\hbar} \int_{-\infty}^{\infty} dt \Im \left\langle \alpha \mathcal{E}(t) \mathcal{E}^\dagger(t) \right\rangle, \tag{5}$$

where $\left\langle n_\omega(t) \right\rangle = Tr[n_\omega(t)\rho(t)]$ and the time derivative has been computed through the Heisenberg equation of motion. Realistically, the signal is a convolution of the nonlinear response and the detector's response function. Thus, the integration in Eq. (5) is restricted by the acceptance width of the spectrometer. Taking advantage of the superoperators formalism in Liouville space [11, 12] and switching to the interaction picture, the stimulated optical signal obtained by a frequency gated measurement is given by [6]

$$S(\omega) = \frac{2}{\hbar} \Im \mathcal{E}_s^*(\omega) \int_{-\infty}^{+\infty} dt\, e^{i\omega t} \left\langle \mathcal{T} P(t) e^{-\frac{i}{\hbar} \int_{-\infty}^{+\infty} dt'\, H'_-(t')} \right\rangle, \tag{6}$$

where $\mathcal{T}$ is the time ordering superoperator, $P(t) = \alpha \sum_i \mathcal{E}_i^\dagger(t)$ is the induced polarization and H'_- is the Liouville superoperator in the interaction picture. We now introduce the perturbative step, expanding the exponential in Eq. (6) to the second order in α:

$$S(\omega) = (-1)^3 \Im \int_{-\infty}^{+\infty} e^{-i\omega t} \mathcal{E}_s^*(\omega) \mathcal{E}_{a/p}(t) \mathcal{T} \prod_{k=1}^{2} \int dt_k \sum_{i,j} \mathcal{E}_i(t_k) \mathcal{E}_j^*(t_k) \left\langle \alpha(t) \alpha(t_1) \alpha(t_2) \right\rangle. \tag{7}$$

This equation fully describes nr-FSRS and is a function of the fifth order nonlinear polarization $P^{(5)}$. The term $\mathcal{E}_{a/p}(t)$ represents alternatively a photon of the actinic or Raman pump pulse: indeed, a last excitation in the form $\alpha \mathcal{E}_s \mathcal{E}_s^\dagger$ leads to a negligible contribution, due to the spectral width of the femtosecond $\mathcal{E}_s$ pulse. Each term in the summation represents a different Liouville pathway and can be sketched by a loop diagram. The number of diagrams can be significantly reduced, considering energy conservation, phase matching and pulses configuration. Therefore, selecting the surviving diagrams simplifies the calculation of the nonlinear signal.

3. Loop diagrams selection

Loop diagrams represent the evolution of the wave function in the joint space of the matter and fields degrees of freedom. Field interactions are represented by pairs of arrows along the two branches of the loop. Interactions with the left or the right side of the loop account for a $\alpha \mathcal{E}_i \mathcal{E}_j^\dagger$ or a $\alpha^\dagger \mathcal{E}_i^\dagger \mathcal{E}_j$ term, respectively. Time flows from bottom to top, thus the two branches are not mutually time ordered, while interactions on the same branch are ordered.

We shall work in frequency domain, by Fourier transforming the field envelopes and defining retarded Green's function $G(\omega) = \frac{1}{\hbar} \sum_\alpha \frac{|\alpha\rangle\langle\alpha|}{\omega - \omega_\alpha + i\gamma}$ and the advanced Green's function $G^\dagger(\omega) = \frac{1}{\hbar} \sum_\alpha \frac{|\alpha\rangle\langle\alpha|}{\omega - \omega_\alpha - i\gamma}$ where $|\alpha\rangle$ is the matter eigenstate basis and γ is the vibrational dephasing rate. Thus, since the polarizability operator can be recast as $\alpha(\omega) = G(\omega)\alpha_{ab}$ where α_{ab} is the dipole constant associated to the transition $a \to b$, we can physically interpret free evolutions on the left and right sides of the diagrams as forwards and backwards in real time, respectively.

The nonlinear response is evaluated considering the possible bare diagrams and dressing them with the fields. Considering actinic excitations at frequencies lower than that of the Raman

pulse and imposing energy conservation we select the relevant diagrams, represented in Fig. 1. Five diagrams contribute to the red side of the spectrum, with respect to the Raman pulse frequency, and five to the blue one. When the delay T between the actinic pulse $\mathcal{E}_a$ and the femtosecond probe pulse $\mathcal{E}_s$ is longer than the pulses duration, the first interaction is necessarily with the actinic field modes and the signal is represented by the four diagrams d_i-d_{iv}. When T is comparable to the femtosecond pulses duration, the nonlinear signal is also generated in the time region in which the three pulses overlap. In this case, the six additional terms d_1-d_6 arise from the summation in Eq. 1. By reading off the diagrams [13], we obtain:

$$S_n(\omega,T) = (-1)^3 P_g \Im \int_{-\infty}^{+\infty} \frac{d\Delta_p}{2\pi}\frac{d\omega'_p}{2\pi}\frac{d\Delta}{2\pi}\frac{d\Delta_a}{2\pi}\frac{d\omega'_a}{2\pi}\, 2\pi\,\delta(\Delta_p-\Delta_a-\Delta)e^{-i\Delta_a T} \\ \mathcal{E}_p(\omega'_p)\mathcal{E}_p^*(\omega'_p+\Delta_p)\mathcal{E}_s(\omega+\Delta)\mathcal{E}_s^*(\omega)\mathcal{E}_a(\omega'_a+\Delta_a)\mathcal{E}_a^*(\omega'_a)F_n(\omega,\Delta,\Delta_p,\omega'_p,\Delta_a,\omega'_a), \quad (8)$$

where the correlation functions F_n depend on the diagram as specified below. The thermal occupation of the state (i) is accounted for through a Boltzmann factor P_i, while the delta function provides energy conservation.

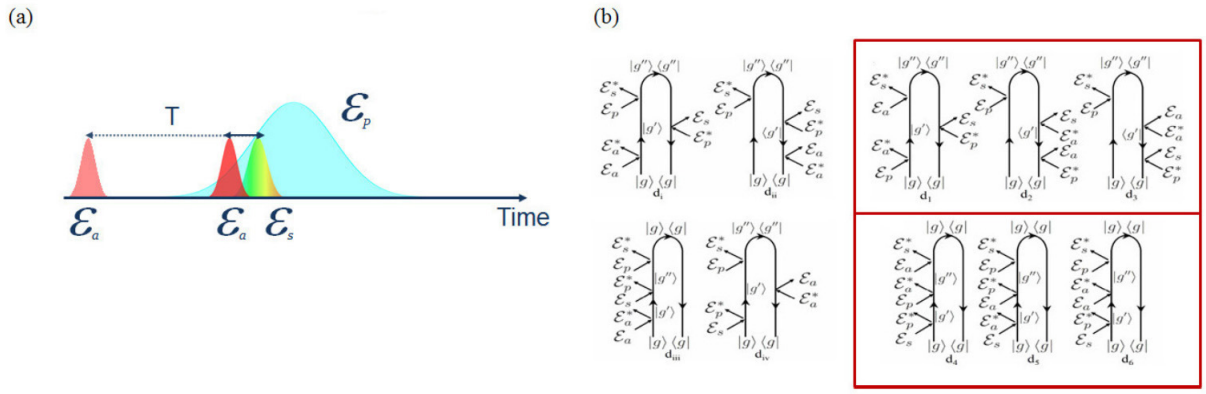

Figure 1: (a) Pulses configuration in nr-FSRS: the actinic pulse triggers a photoinduced process and precedes a couple of Raman pulse and Raman probe fields. When the delay T decreases, the two ultrashort pulses can eventually overlap in time. (b) The total fifth-order signal is represented by ten loop diagrams, five contributions (top panel) in the red side of the spectrum and five (bottom panel) on the blue side. Diagrams that contribute only within the overlap region are highlighted by a red box.

The correlation functions F_n contain the matter response; for diagrams d_i-d_6 we derive

$$F_{d_i} = \left\langle \alpha G^\dagger(\omega'_p-\omega+\Delta_a)\alpha G(\Delta_a)\alpha \right\rangle \qquad F_{d_{ii}} = \left\langle \alpha G^\dagger(\omega'_p-\omega)\alpha G^\dagger(\Delta-\Delta_p)\alpha \right\rangle$$
$$F_{d_{iii}} = \left\langle \alpha G(\Delta_a)\alpha G(\omega+\Delta-\omega'_p-\Delta_p+\Delta_a)\alpha \right\rangle \qquad F_{d_{iv}} = \left\langle \alpha G^\dagger(\Delta-\Delta_p)\alpha G(\omega+\Delta-\omega'_p-\Delta_p)\alpha \right\rangle$$
$$F_{d_1} = \left\langle \alpha G^\dagger(\omega'_p-\omega'_a-\Delta_a)\alpha G(\omega'_p-\omega)\alpha \right\rangle \qquad F_{d_4} = \left\langle \alpha G(\omega-\omega'_a-\Delta_a)\alpha G(\omega-\omega'_p)\alpha \right\rangle$$
$$F_{d_2} = \left\langle \alpha G^\dagger(\omega'_p-\omega)\alpha G^\dagger(\omega'_p-\omega'_a-\Delta_a)\alpha \right\rangle \qquad F_{d_5} = \left\langle \alpha G(\omega-\omega'_p)\alpha G(\omega-\omega'_a-\Delta_a)\alpha \right\rangle$$
$$F_{d_3} = \left\langle \alpha G^\dagger(\omega'_p-\omega)\alpha G^\dagger(\omega'_p-\omega+\Delta_a)\alpha \right\rangle \qquad F_{d_6} = \left\langle \alpha G(\omega-\omega'_p)\alpha G(\omega-\omega'_p-\Delta_a)\alpha \right\rangle .$$

From the analysis of the correlation functions it emerges that diagrams d_i-d_{iv} and d_1-d_6 involve a different set of vibrational modes in order to generate non negligible signals. Remarkably, while

diagrams d_i-d_{iv}, in addition to the probed mode, implicate a low-frequecy mode covered within the bandwidth of the actinic pulse, on the other hand diagrams d_1-d_6 require the presence of an extra level close to frequency difference between the Raman and actinic pulse.

4. Simulations for a model system

Simulations have been performed for a Gaussian actinic pulse centered at 650 nm and with a 50 fs FWHM and we assume a 490 nm monochromatic Raman pulse $\mathcal{E}_p(\omega) = 2\pi\, E_p \delta(\omega - \omega_P)$, which simplifies the frequency domain calculations.
Firstly, we consider a two level molecular system with a low-frequecy mode $\omega_L = 100\,\mathrm{cm}^{-1}$ and a mode $\omega_1 = 1400\,\mathrm{cm}^{-1}$. In this situation, only diagrams d_i-d_{iv}, contribute to the signal: low-frequecy coherences impulsively created by the actinic pump modify the resulting Raman signal, which oscillates from gain to loss features, depending on the time delay T. Depending on the specific pathway, this leads to the creation of main peaks at Raman frequencies as well as side peaks due to harmonic or anharmonic coupling between the modes involved in the process.

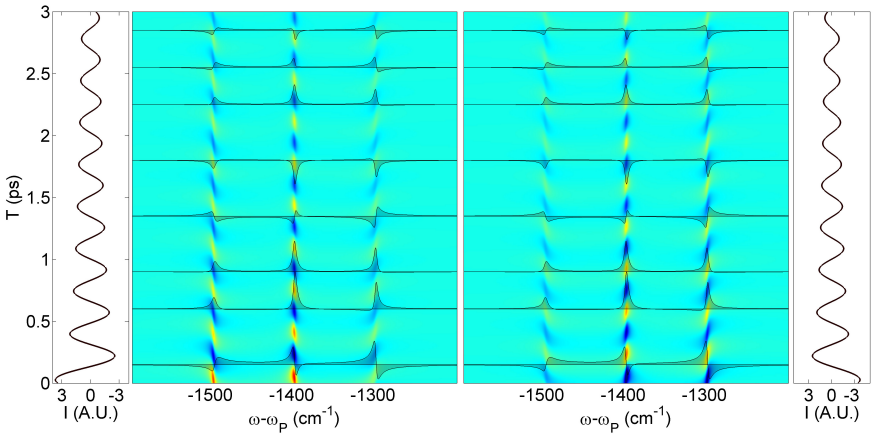

Figure 2: Two dimensional signal $S(\omega, T)$ of diagrams $d_i - d_i v$ for a system with two modes of frequency $\omega_L = 100\,\mathrm{cm}^{-1}$ and $\omega_1 = 1400\,\mathrm{cm}^{-1}$ in the red and the blue sides of the spectrum. The shaded area, which represent the one dimensional signal for selected times, emphasise the oscillation of the signal with T from loss to gain features. The side panels report the integration of the signal over the detected frequency that gives the mean number of photon.

The outcome of the simulations is shown in Fig. 2. The interplay of these features is responsible for a redistribution of photons between the red and the blue sides of the spectrum, as stressed by the side panels in Fig. 2. The total number of photons is conserved but, since red and blue components bring different energies, the total energy flows between fields and matter [14].
Then we consider a two level system, ω_1 and ω_2, with the higher close to the frequency difference between the Raman and the actinic pulse, $\omega_2 = \omega_P - \omega_A$, being ω_P and ω_A the central frequency of Raman and actinic pulse respectively. In this case, diagrams d_1-d_6 contribute for values T comparable to the actinic duration, generating dispersive lineshapes near T=0 and baseline oscillations for negative delays [15]. We show these contributions in Fig. 3.

5. Conclusions

We have introduced a general theoretical description of non resonant impulsive FSRS. In the aim of a full quantum treatment, the relevant perturbative terms contributing to the process have been isolated, tacking advantage of the loop diagram formalism, and the total fifth order

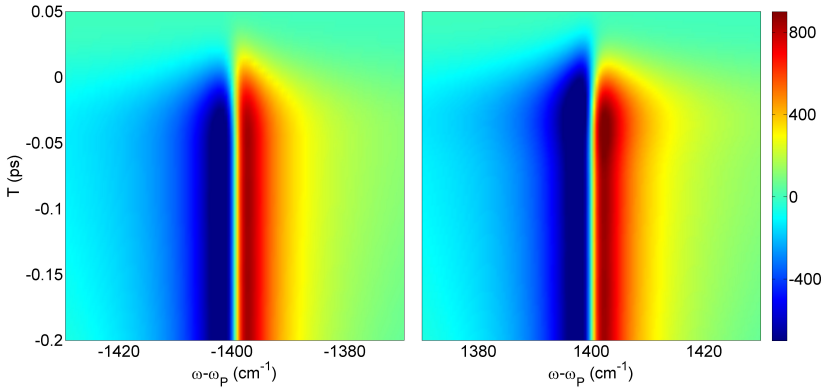

Figure 3: Two dimensional signal $S(\omega, T)$ of diagrams $d_1 - d_6$ for a system with two modes of frequency $\omega_1 = 1400\,\mathrm{cm}^{-1}$ and $\omega_2 = 5030\,\mathrm{cm}^{-1}$ in the red and the blue sides of the spectrum.

response has been calculated. In particular, we investigated the coupling of low and high-frequency modes induced by impulsive actinic excitations and we demonstrated the microscopic mechanism underlying the energy flow between spectral components and matter.
Specifically, the low-frequecy coherences created by the actinic pulse modulate the Raman signals, producing features evolving with the delay T between the actinic and probe pulses. The interplay of these features is responsible for a redistribution of photons between the red and the blue sides of the broadband pulse with respect to the narrowband Raman pulse. Although the total number of photons is conserved during the process, electromagnetic energy is exchanged between the fields and transmitted to the matter degrees of freedom.
Furthermore, we focused on the case of extremely small delays T. When the delay is comparable to the pulses duration, additional signal is generated in the pulse overlap region. This leads to unwanted nonlinear effects which can obscure sample dynamics and have to be taken under control. Indeed, we have found that the optical response in the overlap region of pump and probe fields in nr-FSRS spectroscopy exhibits time dependent features even in the absence of sample dynamics due to the absorption of the pump pulse. The correct evaluation of these contributions is a critical issue for assessing the resolution limit of pump-probe techniques and for future analysis and design of spectroscopic experiments on ultrashort time scales.

References

[1] Provencher F, Bérubé N, Parker A W, Greetham G M, Towrie M, Hellmann C, Côté M, Stingelin N, Silva C and Hayes S C 2014 **5** 4288
[2] Batignani G, Bossini D, Palo N D, Ferrante C, Pontecorvo E, Cerullo G, Kimel A and Scopigno T 2015 *Nature Photonics* **9** 506–10
[3] Kukura P, McCamant D W, Yoon S, Wandschneider D B and Mathies R A 2005 *Science* **310** 1006–9
[4] Fang C, Frontiera R R, Tran R and Mathies R A 2009 *Nature* **462** 200–4
[5] Mukamel S 1995 *Principles of Nonlinear Optical Spectroscopy* (New York: Oxford University Press)
[6] Dorfman K E, Fingerhut B P and Mukamel S 2013 *J. Chem. Phys.* **139** 124113
[7] Rahav S and Mukamel S 2010 *Adv. At., Mol., Opt. Phys.* **59** 223–63
[8] Sun Z, Fu B, Zhang D H and Lee S Y 2009 *The Journal of Chemical Physics* **130** 044312
[9] Kukura P, McCamant D W and Mathies R A 2007 *Annu. Rev. Phys. Chem.* **58** 461–88
[10] Mehlenbacher R D, Lyons B, Wilson K C, Du Y and McCamant D W 2009 *The Journal of Chemical Physics* **131** 244512
[11] Harbola U and Mukamel S 2008 *Phys. Rep.* **465** 191–222
[12] Mukamel S 2003 *Phys. Rev. E* **68** 021111
[13] Biggs J D, Voll J A and Mukamel S 2012 *Phil. Trans. R. Soc. A* **370** 3709–27
[14] Batignani G, Fumero G, Mukamel S and Scopigno T 2015 *Phys. Chem. Chem. Phys.* **17** 10454–61
[15] Fumero G, Batignani G, Dorfman K E, Mukamel S and Scopigno T 2015 *ChemPhysChem* **16** 3438–43